Title

Differential α-Synuclein-induced Autophagy Dysfunction in Neuronal and Microglial Cells drives Tunneling Nanotubes and Aggregate Spread to Microglia

Authors

Ranabir Chakraborty[1,2], Philippa Samella[1,3], Takashi Nonaka[4], Masato Hasegawa[4], Chiara Zurzolo[1,5,*]

Affiliations

[1]Institut Pasteur, Université Paris Cité, CNRS UMR 3691, Membrane Traffic and Pathogenesis, F-75015 Paris, France

[2]Université Paris-Saclay, 91190 Gif-sur-Yvette, France

[3]Trinity College, University of Cambridge, Cambridge, CB2 1TQ, United Kingdom

[4]Dementia Research Project, Tokyo Metropolitan Institute of Medical Science, Tokyo, Japan

[5]Department of Molecular Medicine and Medical Biotechnology, University of Naples Federico II, Naples, Italy

[*]Correspondence: chiara.zurzolo@pasteur.fr

Abstract

Tunneling nanotubes (TNTs) represent a major form of intercellular communication, enabling material exchange of different kinds over long distances between the connected cells. Previous investigations have demonstrated the efficient directional transfer of α-Synuclein (α-Syn) aggregates from neuronal cells to microglia. However, the mechanisms underlying this directional specificity have remained elusive. Here, we investigate the localization, dynamics, and impacts of α-Syn aggregates on the lysosome and autophagic pathways in neuronal and microglial cells. Our findings reveal differential localization of aggregates with lysosomes of neuronal and microglial cells alongside a disparity in lysosomal dynamics. Microglia exhibit a high propensity for lysosomal turnover, particularly through lysophagy, while neuronal lysosomes display compromised degradative capacity and impaired autophagic flux. Consequently, aggregates in neuronal cells are less efficiently targeted for degradation. Furthermore, perturbation of autophagy in neuronal cells elevates TNT-mediated aggregate transfer to microglia. Thus, while revealing distinct effects of α-Syn aggregates in neuronal and microglial cells, our study identifies dysfunctional autophagy as a pivotal determinant driving the preferential directional transfer of aggregates from neurons to microglia.

Teaser

Compromised lysosome functionality and autophagy in neuronal cells leads to α-Synuclein dissipation to microglia via Tunneling Nanotubes.

Graphical Abstract

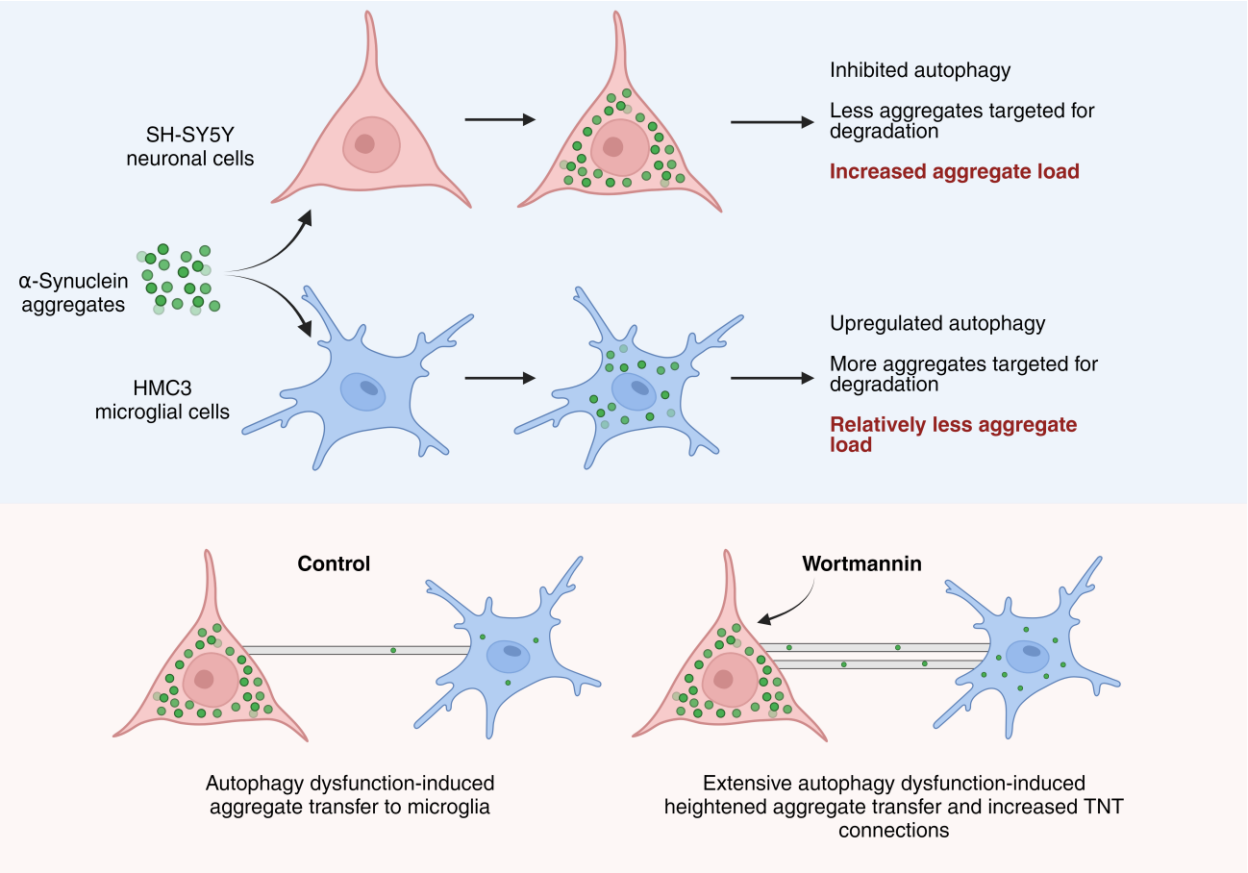

MAIN TEXT

Introduction

Parkinson's Disease (PD) is the second most common neurodegenerative disease, the worldwide burden of which has doubled between 1990 and 2016 (*1*). One of the major genetic associations of sporadic PD, and the first to be discovered, is *SNCA*, which encodes a cytosolic protein α-Synuclein (α-Syn). Both mutations in *SNCA*, as well as elevated levels of the protein (due to duplication and triplication of the gene), can give rise to a pathological state (*2–4*).

A common pathological hallmark of several neurodegenerative diseases, including PD, is disrupted proteostasis. Under physiological conditions, quality control pathways in cells allow for efficient clearing of misfolded proteins, thereby preventing their accumulation and/or aggregation (*5*). Autophagy, a key proteostasis pathway, orchestrates the degradation of obsolete intracellular components, including organelles and aggregated proteins, via lysosomal machinery. Several reports highlight compromised macroautophagy (henceforth referred to as "autophagy") or chaperone-mediated autophagy (CMA) in PD: impaired autophagosome formation (*6*), dysregulated mitophagy due to mutations in genes encoding PTEN-induced putative kinase 1 (*PINK1*) and Parkin RBR E3 ubiquitin-protein ligase (*PARKIN*) (*7*, *8*), decreased CMA caused by mutations in leucine-rich repeat kinase 2 (*LRRK2*) or *SNCA* (*9*, *10*), and impaired lysosomal activity due to mutations in glucocerebrosidase-encoding gene *GBA1* (*11*). Besides genetic mutations, *in vitro* overexpression of α-Syn in human mesencephalic neuronal (LUHMES) cells has also been reported to impair autophagy by preventing the fusion of autophagosomes with lysosomes (*12*). Additionally, overexpression of α-Syn in human neuroblastoma (SH-SY5Y) cells impairs starvation-induced autophagy (*13*). Such dysregulation prompts cells to seek alternative mechanisms to restore homeostasis, failure of which may culminate in apoptosis. Notably, the accumulation of intracellular α-Syn aggregates resulting from dysregulated autophagy has been associated with their secretion via exosomes and membrane shedding (*14–17*). Moreover, recent findings elucidate the role of microglia in alleviating neuronal α-Syn burden through a process termed "synucleinphagy," wherein microglia engulf aggregates released by neurons and target them towards autophagy-mediated clearance (*18*).

However, since their discovery in 2004 (*19*), tunneling nanotubes (TNTs) have emerged as pivotal conduits for contact-dependent cell-to-cell communication that allow for the exchange of various materials, from small ions to larger organelles (*20*). These membranous, F-actin-rich structures also facilitate the movement of neurodegenerative disease-associated protein aggregates such as α-Syn, tau and Amyloid-β (*21*). Notably, α-Syn aggregates exploit TNTs to traverse between diverse cell types, including neuronal precursor cells (NPCs) (*22*), neurons (*23*, *24*), astrocytes (*25*, *26*), and microglia (*27*, *28*). While previous studies have demonstrated the augmentation of homotypic connections between neuronal and microglial cells by α-Syn aggregates, the mechanism underlying their preferential directional transfer from neuronal cells to microglia remains enigmatic. Whether autophagy impairment contributes to the increased connectivity or directionality of aggregate transfer via TNTs remains unexplored.

Through rigorous quantitative microscopy, here we investigate the distinct subcellular dynamics of lysosomal processing abilities in neuronal and microglial cells in the presence and absence of α-Syn aggregates, shedding light on a fundamental imbalance in lysosomal function and autophagy that delineates the preferential transfer of α-Syn aggregates (from neuronal cells) towards microglia.

Results

α-Syn localization in neuronal cells and microglia

To assess the sub-cellular localization of α-Syn pre-formed fibrils, we challenged both SH-SY5Y neuronal and HMC3 microglial cells with the aggregates, and performed immunostaining against early endosome antigen 1 (EEA1) and lysosome-associated membrane protein 1 (LAMP1). We observed a time-dependent increase in the presence of α-Syn with lysosomes, which coincided with a decrease of their localization with early endosomes, a phenotype similar for both the cell types (**Fig. 1**). In neuronal cells, following α-Syn exposure, an average of 20.69% of aggregates localized on early endosomes within 1 hour (1h), declining to 6.92% by the third day after an initial 16h of incubation (72h) (**Fig. 1A and C**). Similarly, in microglia, the proportion of aggregates associated with early endosomes decreased from 20.53% after 1 hour to 4.78% by the final time point assessed (**Fig. 1E and G**). Notably, the occurrence of early endosomes containing aggregates was consistently less than 10% for both the cell types at the two later time points (**Fig. S1A and B**).

Consistent with prior studies (*23*), both SH-SY5Y neuronal cells and HMC3 microglia had higher percentage of aggregates with lysosomes than early endosomes, with this association increasing over time. In SH-SY5Y cells, the proportion of aggregates localized to lysosomes increased from 13.28% after 1 hour of exposure to 89.04% by the final time point (**Fig. 1B and D**). However, microglial lysosomes exhibited a lower α-Syn content relative to neuronal cells, with 14.17% of α-Syn associated with lysosomes after 1 hour, rising to 30.69% after 72 hours of aggregate exposure (**Fig. 1F and H**). Notably, the proportion of lysosomes containing α-Syn decreased over time for both cell types between subsequent time points (**Fig. S1C and D**), with neuronal cells showing a ~9% reduction and microglial lysosomes displaying nearly a 17% decrease in α-Syn content. This divergence in the extent of aggregate association with lysosomes between the two cell types suggests a potential disparity in the impact of aggregates on lysosomal functionality.

α-Syn aggregates differentially affects lysosomes in neuronal cells and microglia

In order to understand the impact of aggregates on lysosomes, we evaluated their degradative ability and motility. Following cell incubation with dye-quenched bovine serum albumin (DQ-BSA), the compound is internalized and trafficked to lysosomes. Catalytic cleavage of the dye results in substantial increase in fluorescence (*29*), thereby allowing to probe the functionality of lysosomes. When treated with the vacuolar ATPase inhibitor bafilomycin A1, which reduces lysosomal pH and consequently impairs their functionality, the fluorescence intensity of DQ-BSA red was significantly lower than the respective controls for both SH-SY5Y and HMC3 cells (**Fig. 2A-C**). Similarly, the presence of aggregates reduced the fluorescence intensity of the dye only after 72h of initial α-Syn exposure in neuronal cells, and not at the earlier time points of 0h (**Fig. 2A upper panels, and B**). Interestingly, in HMC3 cells the response of lysosomes to the presence of aggregates was opposite, with a significant increase in the degradative ability of microglial lysosomes observed over time (**Fig. 2A lower panels, and C**). These results provide a single-cell perspective in the impaired lysosomal functionality of neuronal lysosomes in the presence of aggregates, further supporting the differential impact of aggregates on lysosomes between cell types, wherein microglial lysosomes are more resilient than their neuronal counterparts.

Given the importance of lysosomal trafficking in regulating their position, and consequently their function (*30*), we assessed whether the presence of aggregates on lysosomes influenced their movement. Using lysotracker green we tracked motility at a single lysosome level, over a period of 2 minutes in cells not treated with aggregates (control) or treated with aggregates for 16h following lysosomes containing aggregates (+α-Syn) or not (-α-Syn) (**Fig. 2D-F, Supplementary videos 1-**

6). The presence of aggregates on lysosomes effectively reduced both their mean distance travelled (**Fig. 2G and H**) and their mean velocity (**Fig. 2I and J**). A cumulative frequency distribution also depicts a higher number of lysosomes with reduced distance travelled upon association with α-Syn aggregates (**Fig. S2A and B**). Additionally, the presence of aggregates with lysosomes also caused them to be less motile (distance travelled: 15 μm or less) for both neuronal and microglial cells (**Fig. 2K and L**). Interestingly, the proportion of lysosomes that are less motile is higher in neuronal cells than microglia (34% in neuronal cells versus 14% in microglia in control conditions). The motility of microglial lysosomes was also consistently higher than that of neuronal lysosomes, suggestive of cell type differences in lysosomal trafficking (**Fig. S3D-F**).

Taken together, these data indicate that neuronal lysosomes are more susceptible to the presence of aggregates resulting in compromised degradative capability. Interestingly, the movement of individual lysosomes appears to be equally affected by the presence of aggregates in both neuronal and microglial cells. These observations are consistent with the greater localization of aggregates with lysosomes in neuronal cells (**Fig. 1**), consequently leading to a significant reduction in lysosomal functionality.

α-Syn aggregates differentially affect autophagic flux in neuronal cells and microglia

Having observed the differential effects of α-Syn aggregates on the degradative ability of lysosomes (**Fig. 2A-C**), we investigated their persistence over time. To account for the potential loss of endogenous fluorescence of the aggregates, we immunostained for α-Syn after 1 day (24h) and 3 days (72h) post initial exposure (**Fig. S3A and B**). We observed a significant reduction in the number of aggregates for both neuronal cells and microglia at the two first time points. However, by the third day the extent of reduction was much higher for microglia (62%) compared to neuronal cells (45.38%) (**Fig. S3C and D**), suggestive of differential aggregate clearance ability between the two cell types.

To understand this difference and its underlying mechanism, we investigated whether aggregates had any impact on autophagy, given its reliance on functional lysosomes. Consistent with previous findings of efficient sequestration of α-Syn aggregates by the autophagic pathway in microglia(*18*), we first assessed the potential involvement of autophagy in clearing aggregates within our experimental setup. Both neuronal cells and microglia were incubated with α-Syn aggregates for 6h, followed by autophagy inhibition with bafilomycin A1 for 6 additional hours (**Fig. S4A**). Counting the number of α-Syn puncta per cell revealed accumulation of aggregates upon bafilomycin A1 treatment in both cell types (**Fig. S4B-D**), indicating the importance of autophagy is important in regulating intracellular aggregate load in the experimental conditions used. However, the heightened accumulation of α-Syn in microglial cells compared to neuronal cells (**Fig. S4C and D**) suggests a greater reliance on autophagy for clearing these aggregates in microglia.

The autophagic receptor p62/SQSTM1 (hereafter p62) has been shown to have a central role in aggregate clearance in different neurodegenerative diseases by sequestering cargoes in condensates called p62 bodies, eventually targeting them towards degradation (*31–33*). Notably, in our experimental conditions, exposure to α-Syn in both neuronal cells and microglia for 16 hours led to a significant increase in the number of p62 puncta per cell (**Fig. 3A and C**). However, this augmentation could stem from either an accumulation of p62 (indicative of autophagy flux dysfunction) or an upregulation of the protein itself (suggestive of autophagy flux upregulation). To discern between these possibilities, we treated aggregate-loaded cells with bafilomycin A1, or left them untreated, prior immunostaining for p62. SH-SY5Y cells did not exhibit an elevated number of p62 puncta upon treatment with bafilomycin A1 in the presence of aggregates (**Fig. 3B**),

while a substantial increase was observed for HMC3 cells (**Fig. 3D**). Taken together, these results suggest that autophagy flux is impaired in neuronal cells upon α-Syn exposure, while conversely, is upregulated in microglia.

Having observed a difference in the autophagy flux between the two cell types in the presence of aggregates, we next asked whether these aggregates are targeted towards lysosomes. To assess the extent of aggregate presence in autolysosomes, we co-immunostained for LC3 and LAMP1 (**Fig. 4A**), or for p62 and LAMP1 (**Fig.4B**) and quantified the fraction of cells exhibiting triple localization events (of aggregates with autophagy marker and lysosome), and the number of such events per cell. Both autophagy markers participated in observed events of triple localization (α-Syn-LC3-LAMP1 and α-Syn-p62-LAMP1) in neuronal cells and microglia (**Fig. 4A and B**). Quantification of such events revealed higher percentage of microglia with aggregates in autolysosomes compared to neuronal cells. While over 70% of microglia exhibited triple localization events with both LC3 and p62, the same in neuronal cells was only 26% for LC3, and 35.24% for p62 (**Fig. 4C and E**). In addition, the average number of triple-localized foci per cell was higher in microglia (**Fig. 4D and F**). In line with the data presented above, these results point towards heightened aggregate clearance by autophagy in microglia.

Lysophagy and lysosome biogenesis is elevated in microglia

Given our observation of higher aggregate localization with lysosomes in neuronal cells (**Fig. 1**), along with subsequent disruption of autophagic flux (**Fig. 3**), we hypothesized that the relatively lower persistence of aggregates in microglia could be attributed to a more efficient lysophagic flux in microglia compared to neurons. Since p62 was previously reported to be recruited to damaged lysosomes for lysophagy to occur (*34*), we assessed the extent of colocalization of LAMP1-positive lysosomes with p62 under basal, damaged (with L-leucyl-L-leucine methyl ester [LLOMe]), or α-Syn exposed conditions, in the presence of bafilomycin A1 to identify lysosomes targeted for lysophagy (**Fig. 5A and B**). As expected, the extent of lysosomes undergoing lysophagy was significantly increased upon LLOMe exposure in both neuronal and microglial cells (**Fig. 5C and D**). Aggregate exposure for 16h also increased lysophagy in both the cell types- from a basal level of 6.11% to 13.71% upon aggregate exposure (7.60% increase) in neuronal cells (**Fig. 5C**), and from a basal level of 38.63% to 49.08% in the presence of aggregates (10.45% increase) in microglia (**Fig. 5D**). Interestingly, the fold difference of lysophagy was much higher in microglia than in neuronal cells, both at a basal level, and in the presence of aggregates at different time points (**Fig. 5E**). These results point towards an increased ability of microglia in clearing damaged lysosomes and restoring proteostasis, a process that is less functional in neuronal cells.

As a component of lysophagic flux, clearance of the organelles needs a homeostatic compensation with concomitant lysosomal biogenesis. This is driven by transcription factor EB (TFEB), a major regulator of autophagy and lysosome-associated genes (*35*). We performed immunostaining against TFEB in both neuronal cells and microglia, and assessed the extent of nuclear translocation of the protein. Consistent with our observation of increased lysophagy within 16h of aggregate exposure, the extent of nuclear translocation of TFEB also increases in both the cell types (**Fig. 5F-H**). Considering LAMP1-positive structures as a read-out of TFEB activity, we measured the intensity of LAMP1 per unit area of a cell, and observed a 22% increase for microglia in the presence of aggregates, while only a 7% increase for neuronal cells (**Fig. 5I and J**). Taken together, these results suggest an increase in lysophagy and lysosome biogenesis upon exposure to α-Syn aggregates in both neuronal and microglial cells, with microglia being relatively more efficient in lysosomal turnover and biogenesis.

Inhibited autophagy contributes to increased aggregate transfer, and more TNT connections

Building upon our current data, which revealed dysfunctions in the autophagy pathway in neuronal cells but not in microglia, and upon a previous study demonstrating a directional bias in the transfer of α-Syn aggregates from neuronal cells to microglia (*28*), we formulated the hypothesis that autophagy impairment in neuronal cells could serve as a causal link to the dissipation of aggregates from neurons to microglia. To test this hypothesis, we utilized an irreversible autophagy inhibitor, wortmannin, which selectively inhibits phosphoinositide-3-kinase and prevents autophagosome biogenesis (*36*). SH-SY5Y cells loaded with α-Syn aggregates were treated with wortmannin for 2 hours and then fixed either immediately or after an additional 12 hours of growth in drug-free media. We observed an increased load of aggregates within 2h of wortmannin treatment (1.27-folds higher), which increases even further by 1.42-folds after 12h (**Fig. S5A and C**).

To assess for aggregate transfer, we co-cultured aggregate containing SH-SY5Y cells (N) with acceptor HMC3 cells (M) for 12h in different combinations: wortmannin (Wm) treatment of the donors (N^{Wm}-M), acceptors (N-M^{Wm}), or both (N^{Wm}-M^{Wm}) (**Fig. 6A**). We detected a higher percentage of acceptor microglia containing aggregates in all the conditions of wortmannin treatment compared to control (**Fig. 6B**). As expected, autophagy inhibition in donor neuronal cells increased the extent of transfer to microglia (N^{Wm}-M) by 29.07% compared to control. However, such an increase was also observed when the acceptors were treated with wortmannin (N-M^{Wm}). This could arise from two different possibilities: increased transfer, and/or decreased clearance of aggregates in treated microglia acceptors. To test this, we measured the load of aggregates in microglia immediately after 2h of wortmannin treatment, or after 12h of culture in drug-free media. We observed an elevated load of aggregates in microglia after autophagy inhibition (**Fig. S5B and D**), in line with our previous observation that autophagy is essential for of α-Syn aggregates. Together with our findings of aggregate transfer, the increased detection of α-Syn in N-M^{Wm} group could be due to impaired clearance of aggregates by microglia after receiving them. Importantly, treatment with wortmannin did not result in more exocytosis of aggregates, and the extent of aggregate transfer via secretion was much lower than that observed in co-cultures (**Fig. S5E**).

Upon autophagy inhibition, not only were more acceptor cells positive for aggregates, there was also an increase in the average number of aggregates per acceptor cell (**Fig. 6C**). Compared to the average of 2.89 aggregates per acceptor in control condition, we observe 4.67 aggregates in microglia upon wortmannin treatment of donor cells (N^{Wm}-M). On the other hand, we find an average of 6.27 aggregates in microglia when autophagy was inhibited in the acceptor population (N-M^{Wm}). Interestingly, wortmannin treatment of both the cell populations (N^{Wm}-M^{Wm}) lead to a higher number of aggregates transferred, an average of 11.84.

These results suggest that autophagy dysfunction plays a causal role in the transfer of aggregates from neuronal cells to microglia. As a proof-of-concept that autophagy impairment leads to increased aggregate transfer, we performed a similar experiment, but with microglia serving as the donor cells (**Fig. S6A**). Consistent with our previous results (*28*), in control conditions we observed less transfer of aggregates from microglia to neuronal cells (4.80%), which increased to 13.34% upon autophagy impairment (**Fig. S6B and C**). Wortmannin treatment did not significantly increase the number of aggregates transferred (**Fig. S6D**), which was mildly elevated to an average of 2.35 aggregates per acceptor cell upon autophagy inhibition from a baseline of 2.06 aggregate on average.

As we did not observe any change in the extent of aggregate release via secretion upon wortmannin treatment (**Fig. S5C**), we next assessed if autophagy dysfunction is associated with an increase in TNT connections between cells. After treating both neuronal and microglial cells with wortmannin, we found an increase of 1.83-folds for SH-SY5Y (**Fig. 6D and E**) and of 1.67-folds for HMC3

cells (**Fig. 6F and G**) in the extent of connections. Additionally, upon bafilomycin A1 treatment of cells, the number of connections increased by over 1.5-folds for both the cell types (**Fig. S6E-H**). Taken together, these data suggest that autophagy impairment plays a functional role in contact-mediated α-Syn transfer between neuronal and microglial cells.

Discussion

Several studies have reported that amyloidogenic aggregates can induce the formation of intercellular connections between different cells, facilitating their propagation from one cell to another. After an initial report demonstrating the transfer of the aggregated form of Prion protein (PrP^{Sc}) between CAD neuronal cells, as well as between primary dendritic cells and neurons via TNTs (*37*), subsequent research has shown that various other forms of aggregates including Amyloid-β, Tau, α-Syn, and mutant Huntingtin (mHTT) can also increase intercellular connections, leading to aggregate spread between connected cells (*21*). Such connections are also increased *in vitro* by the small GTPase, Rhes (*38*). Given its enrichment in the striatum, Rhes also facilitates mHTT spread *in vivo* from the striatum to cortical areas (*39*). *In vitro*, α-Syn aggregates can be transferred in a contact dependent manner from mouse neurons to astrocytes with a higher efficiency than in the opposite direction (*26*). Similarly, human neuronal cells are more efficient in transferring α-Syn aggregates to microglia through TNTs than in receiving them (*28*). These *in vitro* and *in vivo* studies collectively point towards a conserved biological phenomenon that allows for neuronal cells to dissipate their aggregate load via TNTs. Our study uncovers a causative role of autophagy dysfunction in inducing TNT-mediated α-Syn aggregate transfer from neuronal cells to microglia. This provides a mechanistic understanding of the directionality of aggregate transfer, while revealing a differential impact of α-Syn aggregates on lysosomal and autophagic pathways between neuronal and microglial cells.

Impaired autophagy is one of the molecular hallmarks of neurodegenerative diseases. Clearance of aggregate-prone proteins such as α-Syn is heavily reliant on autophagy, although the ubiquitin proteasome system can also be involved in the process (*40*, *41*). Notably, inhibition of autophagosome-lysosome fusion using bafilomycin A1 elevates cytotoxicity associated with α-Syn (*42*). This sensitivity to bafilomycin A1 is further supported by the observation of reduced level of synaptosome associated protein 29 (SNAP29), a SNARE protein involved in autophagosome-lysosome fusion, upon transduction of cells with α-Syn (*12*). *In vivo*, in MPTP models of PD, loss of dopaminergic neurons is preceded by lysosomal dysfunction and reduction, with consequent autophagosome accumulation. Such phenotypes are rescued by rapamycin-induced autophagy activation (*43*). A decrease in lysosome-associated markers have also been reported in human PD subjects (*44*). Together with previous findings showing that cells treated with exogenous α-Syn aggregates and PD patient iPSC-derived dopaminergic neurons have impaired lysosomal functions (*23*, *45*), and that lysosomes containing α-Syn are shuttled between cells through TNTs (*23*, *24*), we hypothesized that impairment of autophagy in α-Syn-treated neuronal cells might contribute to the spread of aggregates to neighboring cells via TNTs.

The increased association of aggregates with lysosomes in neuronal cells, (**Fig. 1D and H**), suggests a greater extent of lysosomal damage compared to microglia, corroborated by the reduced degradative ability of neuronal lysosomes, which, on the contrary, increases for microglia (**Fig. 2A-C**). Given their role as resident macrophages of the brain, the heightened functionality of microglial lysosomes in the presence of aggregates is not unexpected. However, it is worth noting that microglial lysosomes have been reported to be being relatively less acidic compared to those of macrophages (*46*, *47*), thereby limiting their degradative ability. The acidity of microglial lysosomes increases in a pro-inflammatory environment, leading to enhanced functionality, as has

been shown in the context of fibrillar amyloid-β clearance (*46*). Similarly, activation of Toll-Like Receptor 2 (TLR2) induces microglial autophagy in both BV2 cells, and *in vivo* mouse models (*48*). Therefore, the observed increased degradative ability of microglial lysosomes in our experiments could be a result of α-Syn-induced pro-inflammatory environment, although further investigations are needed to confirm this hypothesis. Additionally, the observed phenotype in microglia may be attributed to elevated lysosome biogenesis and/or lysosome repair pathways, that lead to a homeostatic maintenance/upregulation of lysosome functionality. Previous research on BV2 microglia demonstrated that upon treatment with fibrillar α-Syn, TANK-Binding Kinase 1 (TBK1) and Optineurin (OPTN) are recruited on lysosomes, facilitating the autophagic clearance of damaged organelles (*49*). Consistent with these findings, we observe elevated lysophagy and concurrent lysosome biogenesis in microglia compared to neuronal cells (**Fig. 5**). This dynamic turnover of lysosomes suggests a mechanism by which microglia are able to counteract the detrimental effects of α-Syn aggregates on lysosomal functionalities. Taken together with our observation of higher aggregate localization on lysosomes, these findings suggest that the extent of lysosomal damage induced by α-Syn is much higher in neuronal cells than in microglia.

Owing to such differences, we hypothesized a differential impact on autophagy between the two cell types. We observed upregulated autophagy in microglia, as opposed to dysfunctional autophagy and accumulation of autophagy substrate p62 in neuronal cells (**Fig. 3**). Additionally, there was an increased co-localization of aggregates with autophagy markers (LC3 and p62) and LAMP1 in microglia (**Fig. 4**). These results corroborate previous findings showing upregulated autophagy in BV2 microglia upon exposure to fibrillar α-Syn (*49*). Taken together, these results suggest that neuronal cells are unable to clear aggregates as efficiently as microglial cells, which is consistent with our observation of a larger fold-decrease of aggregate load in microglia (**Fig. S3**). In conclusion, the observed deficit in autophagy within neuronal cells, coupled with the enhanced autophagic activity in microglia, highlights a critical distinction in the cellular responses to α-Syn aggregates. This deficit in neuronal autophagy may contribute to the impaired clearance of α-Syn aggregates (**Fig. S3**), potentially exacerbating neurodegenerative processes in conditions such as Parkinson's disease.

These findings are also supported by a recent study demonstrating the efficient clearance of neuron-released α-Syn aggregates by microglia in a p62-dependent manner (*18*). The authors also identified a functional link between the toll-like receptor 4 (TLR4)-nuclear factor kappa-light-chain-enhancer of activated B cells (NF-κB) pathway and autophagy-dependent clearance of aggregates. Given that NF-κB is a major transcription factor associated with the production of pro-inflammatory cytokines in the presence of α-Syn pre-formed fibrils (*50*), and is involved in the regulation of autophagy by inducing the expression of associated genes (*51, 52*), it is plausible that the observed upregulation of autophagy in microglia is a consequence of NF-κB activation, regulated upstream by toll-like receptors. This hypothesis, however, remains to be tested. Taken together, these results suggest the need for neuronal cells to find a route dissipate their burden of aggregates.

Given the significant impact of aggregate presence on autophagy within neuronal cells, we hypothesized that this impairment could contribute to the transfer of aggregates to microglial cells (*28*). Inhibition of autophagy in aggregate-laden neuronal cells by wortmannin resulted in a notable increase in aggregate load (**Fig. S5A and C**), and transfer to microglia (**Fig. 6A-C**). Specifically, inhibiting autophagy in donor neuronal cells led to a 29.07% increase in transfer (N^{Wm}-M) compared to the control, indicating the contribution of dysfunctional autophagy to aggregate dissipation to neighbouring cells. On the other hand, the detection of more acceptor cells positive for α-Syn (increase of 27.09% compared to control) upon wortmannin treatment of microglia (N-M^{Wm}) possibly reflects the accumulation of aggregates not targeted for degradation. When both the

cell types were incubated with wortmannin (N^{Wm}-M^{Wm}), no further increase in aggregate transfer was observed compared to the other single cell population treatment groups within the time point of co-culture, suggesting a saturation of aggregate transfer to microglia within the assessed time point of co-culture. However, there was an increase in the number of aggregates transferred when both donors and acceptors were treated with wortmannin (**Fig. 6C**). Assuming a linear relationship between autophagy inhibition and aggregate transfer, a predictive value of average number of aggregates transferred can be obtained by an additive effect of wortmannin on individual cell population (predicted value = 10.94, from N^{Wm}-M + N-M^{Wm} groups), which is close to our observed value of 11.84 (in N^{Wm}-M^{Wm} group). Nevertheless, it is yet to be determined whether there is a bi-directional communication between neuronal cells and microglia that influences the extent of contact-mediated aggregate transfer upon autophagy inhibition. This hypothesis has gained traction from a recent study demonstrating the non-cell autonomous influence of activated microglia in inhibiting neuronal autophagy in Huntington's disease (HD) and tauopathy (*53*). This is achieved by the secretion of proinflammatory chemokines CCL-3/-4/-5 by microglia, which results in neuronal mTORC1 activation, and consequently autophagy inhibition, via the chemokine receptor CCR5. Whether a similar axis operates in the context of Synucleinopathies remains an open question. Additionally, aggregate transfer was also elevated from microglia to neuronal cells upon autophagy inhibition (**S6B-D**). Given our previous observations that the aggregate transfer is relatively weak from microglia to neuronal cells, this increase supports our hypothesis and suggests that autophagy dysfunction serves as a signaling mechanism in intercellular contact-dependent aggregate transfer. Notably, we observed an increase in TNT-connections between both neuronal and microglial cells in the presence of two different autophagy inhibitors targeting distinct steps of the process (**Fig. 6D-G** and **Fig. S6E-H)**. Such an increase, induced by both wortmannin and bafilomycin A1, can be attributed to accumulation of various types of superfluous and unnecessary materials upon autophagy inhibition, triggering a global stress response which promotes TNT formation between cells (*54*). At a mechanistic level, autophagy is closely linked to the endoplasmic reticulum (ER) stress response. Although ER stress is widely associated with upregulated autophagy, it is inhibited in several conditions, such as in neurodegenerative diseases (*55*). Upon activation of ER stress, Ca^{2+} is released into the cytosol via inositol trisphosphate (IP_3) receptor. Elevated cytosolic Ca^{2+} level has previously been reported to positively regulate TNT connections between cells (*56*). Additionally, impairment of autophagosome-lysosome fusion has been reported to cause lysosome membrane permeabilization (LMP) (*57*), resulting in autophagosome accumulation. Intriguingly, such an accumulation was rescued upon treatment with BAPTA-AM, a calcium chelator. These data provide significant promise towards understanding the mechanism of TNT formation as regulated by (dys)functional autophagy, a field that remains largely unexplored.

In conclusion, our study sheds light on the mechanisms underlying elevated aggregate transfer between cells, underscoring the importance of investigating autophagy dysfunction-associated propagation of other aggregate-prone proteins. It also paves way for further research into the role of lysosomes in regulating TNT-mediated interaction between cells, applicable in both physiological and pathological contexts. Importantly, these observations may extend beyond interactions between neuronal and microglial cells, to include neuron-astrocyte communication, which will provide a comprehensive understanding of the biological underpinnings of disease.

Materials and Methods

Culture of Cell lines

Human neuroblastoma cell line SH-SY5Y (referred to as neuronal cells in the manuscript, derived from SK-N-SH neuroblastoma line) were cultured in RPMI1640 media (Euroclone, ECB2000L), and supplemented with 10% foetal calf serum (FCS) (Eurobio Scientific, CVFSVF00-01) and 1% penicillin-streptomycin (Gibco, 15140-122; 100 units/mL final concentration). The human microglia clone 3 cell line (HMC3) were cultured in DMEM (Sigma-Aldrich, D6429) supplemented with 10% FCS and 1% penicillin-streptomycin. Cells were cultured in a humidified CO_2 incubator at 37°C, and passaged using 0.05% Trypsin-EDTA (Gibco, 25300-054) when they reached 90% confluency. Cells were counted before each experiment, and seeded on autoclaved, 12 mm glass coverslips (uncoated) (Epredia, CB00120RA120MNZ0) for fixed-cell imaging, and on 35 mm glass-bottom microdishes (Ibidi GmbH, 81156) for live-cell imaging. Cells between passages 3 and 10 were used for experiments.

Preparation of α-Syn aggregates

α-Syn aggregates were prepared as described before (*58*). Briefly, human wild-type α-Syn was purified from *Escherichia coli* BL21 (DE3) with RP-HPLC. Fibrils were then conjugated with Alexa Fluor™ 488 or 568 fluorophores (used in imaging experiments) (Invitrogen) using manufacturer's labelling kit, or not tagged with a fluorophore. Fibrils were kept at -80°C for long-term storage. Prior to exposure to cells, fibrils were diluted in growth medium at a working concentration of 500 nM and sonicated (BioBlock Scientific, Vibra Cell 7504) for 5 minutes at an amplitude of 80%, pulsed for 5 seconds "on" and 2 seconds "off". Sonicated fibrils were then added on cells directly without the addition of any intracellular delivery agents for 16h. After the designated time periods, cells were washed with diluted trypsin solution (1:3, in 1X DPBS [Gibco, 14040-091]), and allowed to grow further or processed for experiments.

Immunocytochemistry

Immunofluorescence on cells were performed using the standard protocol. Cells were fixed with 4% paraformaldehyde (PFA [Electron Microscopy Sciences, 15710]) for 30 minutes at room temperature (RT), followed by one wash with 1X DPBS. Cells were then incubated in 50 mM ammonium chloride (NH_4Cl [Sigma Aldrich, A0171]) solution for 15 minutes at RT to quench the fixative. Following three washes with 1X DPBS, cells were incubated in 1X DPBS-Tx (0.1% Triton-X100 [Sigma Aldrich, 9002-93-1] in 1X DPBS) for 5 minutes at RT. After three washes with 1X DPBS, cells were incubated in blocking solution of 2% bovine serum albumin (BSA [Sigma Aldrich, A9647]) prepared in 1X DPBS for 1h at RT. Cells were then incubated with primary antibody overnight (for 16h) at 4°C. The following primary antibodies were used: rabbit anti-EEA1 (Thermo Fisher Scientific, PA1-063A; 1:100), mouse anti-LAMP1 (Developmental Studies Hybridoma Bank, H4A3; 1:100), rabbit anti-α-Synuclein (Santa Cruz Biotechnology, sc-7011-R; 1:100), rabbit anti-LC3 (Medical and Biological Laboratories International Corporation, PM036; 1:400), guinea pig anti-p62 (Progen, GP62-C; 1:400), and rabbit anti-TFEB (Cell Signaling Technology, 4240; 1:100). The next day, cells were washed three times with 0.1% DPBS-Tx, followed by incubation with respective secondary antibodies (all from Thermo fisher Scientific, dilution of 1:500 in blocking solution) for 1h at RT. Cells were then washed three times with 1X DPBS, counterstained for nuclei with DAPI (1:1000 in PBS [Sigma-Aldrich, D9542]) and mounted on glass slides with Aqua-Poly/Mount (Polysciences Inc., 18606-20). Slides were imaged at least a day after mounting of coverslips.

Lysosome degradative ability and motility assays

To measure the degradative ability of lysosomes, cells were grown on 35 mm glass-bottom microdishes for 24h, and incubated with 500 nM α-Syn for 16h. Ready-made bafilomycin A1 solution (stock of 0.16 mM- Sigma-Aldrich, SML1661) was diluted to 400 nM in complete medium, and pre-warmed to 37°C before adding to cells for 1h. DQ-BSA Red (Invitrogen, D12051) was diluted in fresh, complete medium to a final concentration of 10 μg/mL, and added to cells for 2h at 37°C. Cells were thoroughly washed with complete medium before imaging.

To assess the motility of lysosomes, cells were incubated for 16h with α-Syn aggregates conjugated with AlexaFluor 568 fluorophore. After a thorough wash with 1:3 diluted trypsin, cells were incubated with 500 nM Lysotracker Green DND-189 (Thermo Fisher Scientific, L7535) diluted in fresh, complete medium for 30 minutes at 37°C. After a wash with complete medium, fresh phenol red-free RPMI 1640 medium (for SH-SY5Y cells) and FluoroBrite™ DMEM (for HMC3 cells) was added and the dishes were incubated in a 37°C, 5% CO_2, 50% relative humidity environmental chamber equipped with the microscope. Time-lapse imaging was performed using Nikon Eclipse Ti2 microscope with a spinning disk confocal set-up (Yokogawa) with the following lasers (wavelength in nm): 405, 488, 561 and 640 nm. Cells were imaged using a 100X oil immersion objective (1.45 numerical aperture) for 5 minutes. 5 optical sections of 1 μm interval (± 2 sections from the middle plane) were taken for each frame in two wavelengths- 488 nm and 561 nm. Each acquisition was made at a time interval of 1.537 seconds.

Autophagy and lysophagy flux analysis

To assess autophagy flux upon exposure of cells to α-Syn aggregates, cells were immunostained for p62 (as previously described). For bafilomycin treatment of α-Syn containing cells, 400 nM of the drug was added to cells in the fifteenth hour (last 1h of aggregate incubation), followed by fixation. For lysophagy analysis, similar approach was undertaken for aggregate and bafilomycin A1 incubation. Lysophagy was induced by the lysosome-damaging drug L-leucyl-L-leucine methyl ester (LLOMe; Sigma-Aldrich, L7393) at a concentration of 1 mM for 1h, co-incubated with bafilomycin A1. Cells were then washed with 1X DPBS, and processed for immunocytochemistry.

α-Syn transfer assay

To assess for aggregate transfer, neuronal cells or microglia were grown for 24h in a 6-well dish, and then exposed to 500 nM of α-Syn aggregates, prepared as previously described. After 16h of incubation, cells (now the donor population) were trypsinized and seeded on 12 mm coverslips. After 22h post-seeding, donor cells were treated (or not) with 200 nM wortmannin (Sigma Aldrich, W1628) for 2h. Cells were then washed with complete media once, and then fresh media was added. At this point, microglia or neuronal cells (acceptor population) were added to the culture (1:1 ratio). For the experiment wherein both donor and acceptor cell populations were treated with wortmannin, the donor population was seeded first on coverslips, and grown for 22h. Media was replaced and the acceptor population was added, along with wortmannin. Media was replaced after 2h of wortmannin treatment. Co-cultures were done for 12h, after which cells were fixed to preserve TNTs (described below) and stained with wheat germ agglutinin 647 (WGA, Thermo Fisher Scientific, W32466; 3.33 μg/mL) for 15 minutes at RT, followed by nuclei counterstaining with DAPI (1:1000 in 1X DPBS).

To assess the extent of secretion-mediated aggregate transfer, conditioned media from aggregate containing cells treated (or not) with wortmannin was added to acceptor microglia for 12h. Data represented is normalized to secretion control (data from secretion control subtracted from the co-culture data).

TNT counting

To efficiently visualize TNTs in cultures, cells were fixed at sub-confluency (~70%). In order to appropriately preserve TNTs, two different fixative solutions were used, as described previously (*28*, *59*): fixative 1 (0.05% glutaraldehyde [GA {Sigma Aldrich, G5882}], 2% PFA, 0.2 M HEPES buffer [Gibco, 15630-080] in 1X DPBS), followed by fixative 2 (4% PFA, 0.2 M HEPES buffer in 1X DPBS) for 15 minutes each at RT. Cells were then labelled with Phalloidin 647 (Thermo Fisher Scientific, A12380; 1:250 in 1X DPBS) and DAPI (1:1000 in 1X DPBS) for 15 minutes each at RT. Cells were then washed once with 1X DPBS and mounted on glass slides.

Fixed-cell microscopy

Images were acquired using Zeiss LSM900 inverted confocal microscope equipped with four lasers (wavelength in nm): 405, 488, 561 and 640 nm. For TNT counting, samples were imaged using 40X oil immersion objective (1.3 numerical aperture) with a field-of-view effective zoom of 0.8x, whereas all other immunofluorescence samples were acquired using a 63X oil immersion objective (1.4 numerical aperture) with a 1x zoom. Image acquisition was performed using ZEN blue software. The entire cell volume was imaged for all samples, with optical sections of 0.45 μm. Depending on the cell types, the entire volume of cells ranged between 7 and 13 μm in thickness.

Quantification and Statistical Analyses

For TNT counting, images were processed for analysis using the "manual TNT annotation" plug-in of ICY software (https://icy.bioimageanalysis.org/plugin/manual-tnt-annotation/). Number of p62 puncta or α-Syn aggregates per cell were manually counted in 3D images, through the z-stacks. Colocalization analysis was performed using the JACoP plug-in FIJI (*60*). 3D images were used for colocalizing two channels with object-based detection, and thresholding of objects was performed manually. Triple colocalization events were counted manually for each cell in 3D images. Imaris 9.9.1 (Oxford instruments) software was used to create spots for 3D rendering of confocal-acquired images. Time-lapse videos were analyzed for ~2 minutes (80 frames) to track lysosomal motility. Manual tracking was performed using the FIJI plug-in MTrackJ (*61*) for single lysosomes. Only those lysosomes were tracked that were not in the perinuclear area, and that remained within the region of interest for the entire duration of tracking without merging/interacting with other lysosomes. Movies were then created at a frame speed of 5 fps.

No prior power analysis was done to measure the sample size. Graphs were plotted using GraphPad prism 10.0, and appropriate statistical tests were performed on raw data, and not on fold-change normalized data. Statistical tests performed are mentioned within the figure legends. All the experiments were performed for three independent biological replicates.

References

1. E. R. Dorsey, A. Elbaz, E. Nichols, N. Abbasi, F. Abd-Allah, A. Abdelalim, J. C. Adsuar, M. G. Ansha, C. Brayne, J.-Y. J. Choi, D. Collado-Mateo, N. Dahodwala, H. P. Do, D. Edessa, M. Endres, S.-M. Fereshtehnejad, K. J. Foreman, F. G. Gankpe, R. Gupta, S. Hamidi, G. J. Hankey, S. I. Hay, M. I. Hegazy, D. T. Hibstu, A. Kasaeian, Y. Khader, I. Khalil, Y.-H. Khang, Y. J. Kim, Y. Kokubo, G. Logroscino, J. Massano, N. Mohamed Ibrahim, M. A. Mohammed, A. Mohammadi, M. Moradi-Lakeh, M. Naghavi, B. T. Nguyen, Y. L. Nirayo, F. A. Ogbo, M. O. Owolabi, D. M. Pereira, M. J. Postma, M. Qorbani, M. A. Rahman, K. T. Roba, H. Safari, S. Safiri, M. Satpathy, M. Sawhney, A. Shafieesabet, M. S. Shiferaw, M. Smith, C. E. I. Szoeke, R. Tabarés-Seisdedos, N. T. Truong, K. N. Ukwaja, N. Venketasubramanian, S. Villafaina, K. G. Weldegwergs, R. Westerman, T. Wijeratne, A. S. Winkler, B. T. Xuan, N. Yonemoto, V. L. Feigin, T. Vos, C. J. L. Murray, Global, regional, and national burden of Parkinson's disease, 1990–2016: a systematic analysis for the Global Burden of Disease Study 2016. *The Lancet Neurology* **17**, 939–953 (2018).
2. M. H. Polymeropoulos, C. Lavedan, E. Leroy, S. E. Ide, A. Dehejia, A. Dutra, B. Pike, H. Root, J. Rubenstein, R. Boyer, E. S. Stenroos, S. Chandrasekharappa, A. Athanassiadou, T. Papapetropoulos, W. G. Johnson, A. M. Lazzarini, R. C. Duvoisin, G. Di Iorio, L. I. Golbe, R. L. Nussbaum, Mutation in the α-Synuclein Gene Identified in Families with Parkinson's Disease. *Science* **276**, 2045–2047 (1997).
3. A. B. Singleton, M. Farrer, J. Johnson, A. Singleton, S. Hague, J. Kachergus, M. Hulihan, T. Peuralinna, A. Dutra, R. Nussbaum, S. Lincoln, A. Crawley, M. Hanson, D. Maraganore, C. Adler, M. R. Cookson, M. Muenter, M. Baptista, D. Miller, J. Blancato, J. Hardy, K. Gwinn-Hardy, α-Synuclein Locus Triplication Causes Parkinson's Disease. *Science* **302**, 841–841 (2003).
4. D. W. Miller, S. M. Hague, J. Clarimon, M. Baptista, K. Gwinn-Hardy, M. R. Cookson, A. B. Singleton, α-Synuclein in blood and brain from familial Parkinson disease with SNCA locus triplication. *Neurology* **62**, 1835–1838 (2004).
5. W. E. Balch, R. I. Morimoto, A. Dillin, J. W. Kelly, Adapting proteostasis for disease intervention. *Science* **319**, 916–919 (2008).
6. A. R. Winslow, C.-W. Chen, S. Corrochano, A. Acevedo-Arozena, D. E. Gordon, A. A. Peden, M. Lichtenberg, F. M. Menzies, B. Ravikumar, S. Imarisio, S. Brown, C. J. O'Kane, D. C. Rubinsztein, α-Synuclein impairs macroautophagy: implications for Parkinson's disease. *Journal of Cell Biology* **190**, 1023–1037 (2010).
7. E. M. Valente, P. M. Abou-Sleiman, V. Caputo, M. M. K. Muqit, K. Harvey, S. Gispert, Z. Ali, D. Del Turco, A. R. Bentivoglio, D. G. Healy, A. Albanese, R. Nussbaum, R. González-Maldonado, T. Deller, S. Salvi, P. Cortelli, W. P. Gilks, D. S. Latchman, R. J. Harvey, B. Dallapiccola, G. Auburger, N. W. Wood, Hereditary Early-Onset Parkinson's Disease Caused by Mutations in PINK1. *Science* **304**, 1158–1160 (2004).
8. T. Kitada, S. Asakawa, N. Hattori, H. Matsumine, Y. Yamamura, S. Minoshima, M. Yokochi, Y. Mizuno, N. Shimizu, Mutations in the parkin gene cause autosomal recessive juvenile parkinsonism. *Nature* **392**, 605–608 (1998).
9. S. J. Orenstein, S.-H. Kuo, I. Tasset, E. Arias, H. Koga, I. Fernandez-Carasa, E. Cortes, L. S. Honig, W. Dauer, A. Consiglio, A. Raya, D. Sulzer, A. M. Cuervo, Interplay of LRRK2 with chaperone-mediated autophagy. *Nat Neurosci* **16**, 394–406 (2013).
10. L. Alvarez-Erviti, M. C. Rodriguez-Oroz, J. M. Cooper, C. Caballero, I. Ferrer, J. A. Obeso, A. H. V. Schapira, Chaperone-Mediated Autophagy Markers in Parkinson Disease Brains. *Archives of Neurology* **67**, 1464–1472 (2010).
11. S. P. Sardi, J. Clarke, C. Kinnecom, T. J. Tamsett, L. Li, L. M. Stanek, M. A. Passini, G. A. Grabowski, M. G. Schlossmacher, R. L. Sidman, S. H. Cheng, L. S. Shihabuddin, CNS expression of glucocerebrosidase corrects α-synuclein pathology and memory in a mouse model of Gaucher-related synucleinopathy. *Proceedings of the National Academy of Sciences* **108**, 12101–12106 (2011).
12. Q. Tang, P. Gao, T. Arzberger, M. Höllerhage, J. Herms, G. Höglinger, T. Koeglsperger, Alpha-Synuclein defects autophagy by impairing SNAP29-mediated autophagosome-lysosome fusion. *Cell Death Dis* **12**, 1–16 (2021).
13. A. C. Nascimento, A. G. Erustes, P. Reckziegel, C. Bincoletto, R. P. Ureshino, G. J. S. Pereira, S. S. Smaili, α-Synuclein Overexpression Induces Lysosomal Dysfunction and Autophagy Impairment in Human Neuroblastoma SH-SY5Y. *Neurochem Res* **45**, 2749–2761 (2020).
14. L. Alvarez-Erviti, Y. Seow, A. H. Schapira, C. Gardiner, I. L. Sargent, M. J. A. Wood, J. M. Cooper, Lysosomal dysfunction increases exosome-mediated alpha-synuclein release and transmission. *Neurobiology of Disease* **42**, 360–367 (2011).
15. K. M. Danzer, L. R. Kranich, W. P. Ruf, O. Cagsal-Getkin, A. R. Winslow, L. Zhu, C. R. Vanderburg, P. J. McLean, Exosomal cell-to-cell transmission of alpha synuclein oligomers. *Molecular Neurodegeneration* **7**, 42 (2012).
16. H.-J. Lee, E.-D. Cho, K. W. Lee, J.-H. Kim, S.-G. Cho, S.-J. Lee, Autophagic failure promotes the exocytosis and intercellular transfer of α-synuclein. *Exp Mol Med* **45**, e22–e22 (2013).

17. A.-M. Poehler, W. Xiang, P. Spitzer, V. E. L. May, H. Meixner, E. Rockenstein, O. Chutna, T. F. Outeiro, J. Winkler, E. Masliah, J. Klucken, Autophagy modulates SNCA/α-synuclein release, thereby generating a hostile microenvironment. *Autophagy* **10**, 2171–2192 (2014).
18. I. Choi, Y. Zhang, S. P. Seegobin, M. Pruvost, Q. Wang, K. Purtell, B. Zhang, Z. Yue, Microglia clear neuron-released α-synuclein via selective autophagy and prevent neurodegeneration. *Nat Commun* **11**, 1386 (2020).
19. A. Rustom, R. Saffrich, I. Markovic, P. Walther, H.-H. Gerdes, Nanotubular Highways for Intercellular Organelle Transport. *Science* **303**, 1007–1010 (2004).
20. D. Cordero Cervantes, C. Zurzolo, Peering into tunneling nanotubes—The path forward. *The EMBO Journal* **40**, e105789 (2021).
21. R. Chakraborty, S. Belian, C. Zurzolo, Hijacking intercellular trafficking for the spread of protein aggregates in neurodegenerative diseases: a focus on tunneling nanotubes (TNTs). *Extracell Vesicles Circ Nucleic Acids* **4**, 27–43 (2023).
22. C. Grudina, G. Kouroupi, T. Nonaka, M. Hasegawa, R. Matsas, C. Zurzolo, Human NPCs can degrade α–syn fibrils and transfer them preferentially in a cell contact-dependent manner possibly through TNT-like structures. *Neurobiology of Disease* **132**, 104609 (2019).
23. A. D. Senol, M. Samarani, S. Syan, C. M. Guardia, T. Nonaka, N. Liv, P. Latour-Lambert, M. Hasegawa, J. Klumperman, J. S. Bonifacino, C. Zurzolo, α-Synuclein fibrils subvert lysosome structure and function for the propagation of protein misfolding between cells through tunneling nanotubes. *PLOS Biology* **19**, e3001287 (2021).
24. S. Abounit, L. Bousset, F. Loria, S. Zhu, F. de Chaumont, L. Pieri, J.-C. Olivo-Marin, R. Melki, C. Zurzolo, Tunneling nanotubes spread fibrillar α-synuclein by intercellular trafficking of lysosomes. *The EMBO Journal* **35**, 2120–2138 (2016).
25. J. Rostami, S. Holmqvist, V. Lindström, J. Sigvardson, G. T. Westermark, M. Ingelsson, J. Bergström, L. Roybon, A. Erlandsson, Human Astrocytes Transfer Aggregated Alpha-Synuclein via Tunneling Nanotubes. *J. Neurosci.* **37**, 11835–11853 (2017).
26. F. Loria, J. Y. Vargas, L. Bousset, S. Syan, A. Salles, R. Melki, C. Zurzolo, α-Synuclein transfer between neurons and astrocytes indicates that astrocytes play a role in degradation rather than in spreading. *Acta Neuropathol* **134**, 789–808 (2017).
27. H. Scheiblich, C. Dansokho, D. Mercan, S. V. Schmidt, L. Bousset, L. Wischhof, F. Eikens, A. Odainic, J. Spitzer, A. Griep, S. Schwartz, D. Bano, E. Latz, R. Melki, M. T. Heneka, Microglia jointly degrade fibrillar alpha-synuclein cargo by distribution through tunneling nanotubes. *Cell* **184**, 5089-5106.e21 (2021).
28. R. Chakraborty, T. Nonaka, M. Hasegawa, C. Zurzolo, Tunnelling nanotubes between neuronal and microglial cells allow bi-directional transfer of α-Synuclein and mitochondria. *Cell Death Dis* **14**, 1–12 (2023).
29. R. Marwaha, M. Sharma, DQ-Red BSA Trafficking Assay in Cultured Cells to Assess Cargo Delivery to Lysosomes. *BIO-PROTOCOL* **7** (2017).
30. G. Scerra, V. De Pasquale, M. Scarcella, M. G. Caporaso, L. M. Pavone, M. D'Agostino, Lysosomal positioning diseases: beyond substrate storage. *Open Biology* **12**, 220155 (2022).
31. E. Kuusisto, A. Salminen, I. Alafuzoff, Ubiquitin-binding protein p62 is present in neuronal and glial inclusions in human tauopathies and synucleinopathies. *NeuroReport* **12**, 2085 (2001).
32. G. Bjørkøy, T. Lamark, A. Brech, H. Outzen, M. Perander, A. Øvervatn, H. Stenmark, T. Johansen, p62/SQSTM1 forms protein aggregates degraded by autophagy and has a protective effect on huntingtin-induced cell death. *Journal of Cell Biology* **171**, 603–614 (2005).
33. S. Pankiv, T. H. Clausen, T. Lamark, A. Brech, J.-A. Bruun, H. Outzen, A. Øvervatn, G. Bjørkøy, T. Johansen, p62/SQSTM1 Binds Directly to Atg8/LC3 to Facilitate Degradation of Ubiquitinated Protein Aggregates by Autophagy *. *Journal of Biological Chemistry* **282**, 24131–24145 (2007).
34. E. R. Gallagher, E. L. F. Holzbaur, The selective autophagy adaptor p62/SQSTM1 forms phase condensates regulated by HSP27 that facilitate the clearance of damaged lysosomes via lysophagy. *Cell Reports* **42**, 112037 (2023).
35. C. Settembre, C. Di Malta, V. A. Polito, M. G. Arencibia, F. Vetrini, S. Erdin, S. U. Erdin, T. Huynh, D. Medina, P. Colella, M. Sardiello, D. C. Rubinsztein, A. Ballabio, TFEB Links Autophagy to Lysosomal Biogenesis. *Science* **332**, 1429–1433 (2011).
36. E. F. C. Blommaart, U. Krause, J. P. M. Schellens, H. Vreeling-Sindelárová, A. J. Meijer, The Phosphatidylinositol 3-Kinase Inhibitors Wortmannin and LY294002 Inhibit Autophagy in Isolated Rat Hepatocytes. *European Journal of Biochemistry* **243**, 240–246 (1997).
37. K. Gousset, E. Schiff, C. Langevin, Z. Marijanovic, A. Caputo, D. T. Browman, N. Chenouard, F. de Chaumont, A. Martino, J. Enninga, J.-C. Olivo-Marin, D. Männel, C. Zurzolo, Prions hijack tunnelling nanotubes for intercellular spread. *Nat Cell Biol* **11**, 328–336 (2009).
38. M. Sharma, S. Subramaniam, Rhes travels from cell to cell and transports Huntington disease protein via TNT-like protrusion. *Journal of Cell Biology* **218**, 1972–1993 (2019).
39. U. N. Ramírez-Jarquín, M. Sharma, N. Shahani, Y. Li, S. Boregowda, S. Subramaniam, Rhes protein transits from neuron to neuron and facilitates mutant huntingtin spreading in the brain. *Science Advances* **8**, eabm3877 (2022).

40. J. L. Webb, B. Ravikumar, J. Atkins, J. N. Skepper, D. C. Rubinsztein, α-Synuclein Is Degraded by Both Autophagy and the Proteasome*. *Journal of Biological Chemistry* **278**, 25009–25013 (2003).
41. T. Vogiatzi, M. Xilouri, K. Vekrellis, L. Stefanis, Wild Type α-Synuclein Is Degraded by Chaperone-mediated Autophagy and Macroautophagy in Neuronal Cells*. *Journal of Biological Chemistry* **283**, 23542–23556 (2008).
42. J. Klucken, A.-M. Poehler, D. Ebrahimi-Fakhari, J. Schneider, S. Nuber, E. Rockenstein, U. Schlötzer-Schrehardt, B. T. Hyman, P. J. McLean, E. Masliah, J. Winkler, Alpha-synuclein aggregation involves a bafilomycin A1-sensitive autophagy pathway. *Autophagy* **8**, 754–766 (2012).
43. B. Dehay, J. Bové, N. Rodríguez-Muela, C. Perier, A. Recasens, P. Boya, M. Vila, Pathogenic Lysosomal Depletion in Parkinson's Disease. *J. Neurosci.* **30**, 12535–12544 (2010).
44. Y. Chu, H. Dodiya, P. Aebischer, C. W. Olanow, J. H. Kordower, Alterations in lysosomal and proteasomal markers in Parkinson's disease: Relationship to alpha-synuclein inclusions. *Neurobiology of Disease* **35**, 385–398 (2009).
45. A. Drobny, F. A. Boros, D. Balta, S. Prieto Huarcaya, D. Caylioglu, N. Qazi, J. Vandrey, Y. Schneider, J. P. Dobert, C. Pitcairn, J. R. Mazzulli, F. Zunke, Reciprocal effects of alpha-synuclein aggregation and lysosomal homeostasis in synucleinopathy models. *Translational Neurodegeneration* **12**, 31 (2023).
46. A. Majumdar, D. Cruz, N. Asamoah, A. Buxbaum, I. Sohar, P. Lobel, F. R. Maxfield, Activation of Microglia Acidifies Lysosomes and Leads to Degradation of Alzheimer Amyloid Fibrils. *MBoC* **18**, 1490–1496 (2007).
47. J. D. Quick, C. Silva, J. H. Wong, K. L. Lim, R. Reynolds, A. M. Barron, J. Zeng, C. H. Lo, Lysosomal acidification dysfunction in microglia: an emerging pathogenic mechanism of neuroinflammation and neurodegeneration. *Journal of Neuroinflammation* **20**, 185 (2023).
48. D. S. Arroyo, J. A. Soria, E. A. Gaviglio, C. Garcia-Keller, L. M. Cancela, M. C. Rodriguez-Galan, J. M. Wang, P. Iribarren, Toll-like receptor 2 ligands promote microglial cell death by inducing autophagy. *The FASEB Journal* **27**, 299–312 (2013).
49. C. Bussi, J. M. Peralta Ramos, D. S. Arroyo, J. I. Gallea, P. Ronchi, A. Kolovou, J. M. Wang, O. Florey, M. S. Celej, Y. Schwab, N. T. Ktistakis, P. Iribarren, Alpha-synuclein fibrils recruit TBK1 and OPTN to lysosomal damage sites and induce autophagy in microglial cells. *Journal of Cell Science* **131**, jcs226241 (2018).
50. D. Dutta, M. Jana, M. Majumder, S. Mondal, A. Roy, K. Pahan, Selective targeting of the TLR2/MyD88/NF-κB pathway reduces α-synuclein spreading in vitro and in vivo. *Nat Commun* **12**, 5382 (2021).
51. M. Nivon, E. Richet, P. Codogno, A.-P. Arrigo, C. Kretz-Remy, Autophagy activation by NFκB is essential for cell survival after heat shock. *Autophagy* **5**, 766–783 (2009).
52. T. Copetti, C. Bertoli, E. Dalla, F. Demarchi, C. Schneider, p65/RelA Modulates BECN1 Transcription and Autophagy. *Molecular and Cellular Biology* **29**, 2594–2608 (2009).
53. B. P. Festa, F. H. Siddiqi, M. Jimenez-Sanchez, H. Won, M. Rob, A. Djajadikerta, E. Stamatakou, D. C. Rubinsztein, Microglial-to-neuronal CCR5 signaling regulates autophagy in neurodegeneration. *Neuron* **111**, 2021-2037.e12 (2023).
54. G. Kroemer, G. Mariño, B. Levine, Autophagy and the Integrated Stress Response. *Molecular Cell* **40**, 280–293 (2010).
55. H.-O. Rashid, R. K. Yadav, H.-R. Kim, H.-J. Chae, ER stress: Autophagy induction, inhibition and selection. *Autophagy* **11**, 1956–1977 (2015).
56. J. Y. Vargas, F. Loria, Y. Wu, G. Córdova, T. Nonaka, S. Bellow, S. Syan, M. Hasegawa, G. M. van Woerden, C. Trollet, C. Zurzolo, The Wnt/Ca2+ pathway is involved in interneuronal communication mediated by tunneling nanotubes. *The EMBO Journal* **38**, e101230 (2019).
57. P. Hu, J. Wang, Y. Qing, H. Li, W. Sun, X. Yu, H. Hui, Q. Guo, J. Xu, FV-429 induces autophagy blockage and lysosome-dependent cell death of T-cell malignancies via lysosomal dysregulation. *Cell Death Dis* **12**, 1–14 (2021).
58. T. Nonaka, S. T. Watanabe, T. Iwatsubo, M. Hasegawa, Seeded Aggregation and Toxicity of α-Synuclein and Tau: CELLULAR MODELS OF NEURODEGENERATIVE DISEASES*. *Journal of Biological Chemistry* **285**, 34885–34898 (2010).
59. I. Sáenz-de-Santa-María, J. M. Henderson, A. Pepe, C. Zurzolo, Identification and Characterization of Tunneling Nanotubes for Intercellular Trafficking. *Current Protocols* **3**, e939 (2023).
60. S. Bolte, F. P. Cordelières, A guided tour into subcellular colocalization analysis in light microscopy. *Journal of Microscopy* **224**, 213–232 (2006).
61. E. Meijering, O. Dzyubachyk, I. Smal, "Methods for Cell and Particle Tracking" in *Methods in Enzymology* (Elsevier, 2012; https://linkinghub.elsevier.com/retrieve/pii/B9780123918574000094)vol. 504, pp. 183–200.

Acknowledgments

We thank all the members of the Membrane Traffic and Pathogenesis Unit, Institut Pasteur, for insightful discussions, Francesca Palese and Sevan Belian for critical reading of the manuscript. We thank Reine Bouyssie, a member of the administrative staff of the Membrane Traffic and Pathogenesis Unit for her continued support.

Funding:

Pasteur-Paris University International Doctoral Program (RC)
Biology Summer Studentship Programme - Institut Pasteur and Trinity College, University of Cambridge (PS)
France Parkinson - Soutien de l'Association France Parkinson 2021 (CZ)
Don Explore AD - Programme Explore de l'Institut Pasteur (CZ)
Agence Nationale de la Recherche ANR-20-CE13-0032-01 (CZ)
Fondation pour la Recherche Médicale FRM - EQU202103012630 (CZ)

Author contributions:

Conceptualization: RC, CZ
Methodology: RC, PS, TN, MH
Investigation: RC, PS
Visualization: RC
Supervision: CZ
Writing—original draft: RC
Writing—review & editing: RC, PS, CZ

Competing interests:

Authors declare that there are no competing interests.

Data and materials availability:

All data are available in the main text, or in the supplementary materials.

Figures and Tables

Figure 1

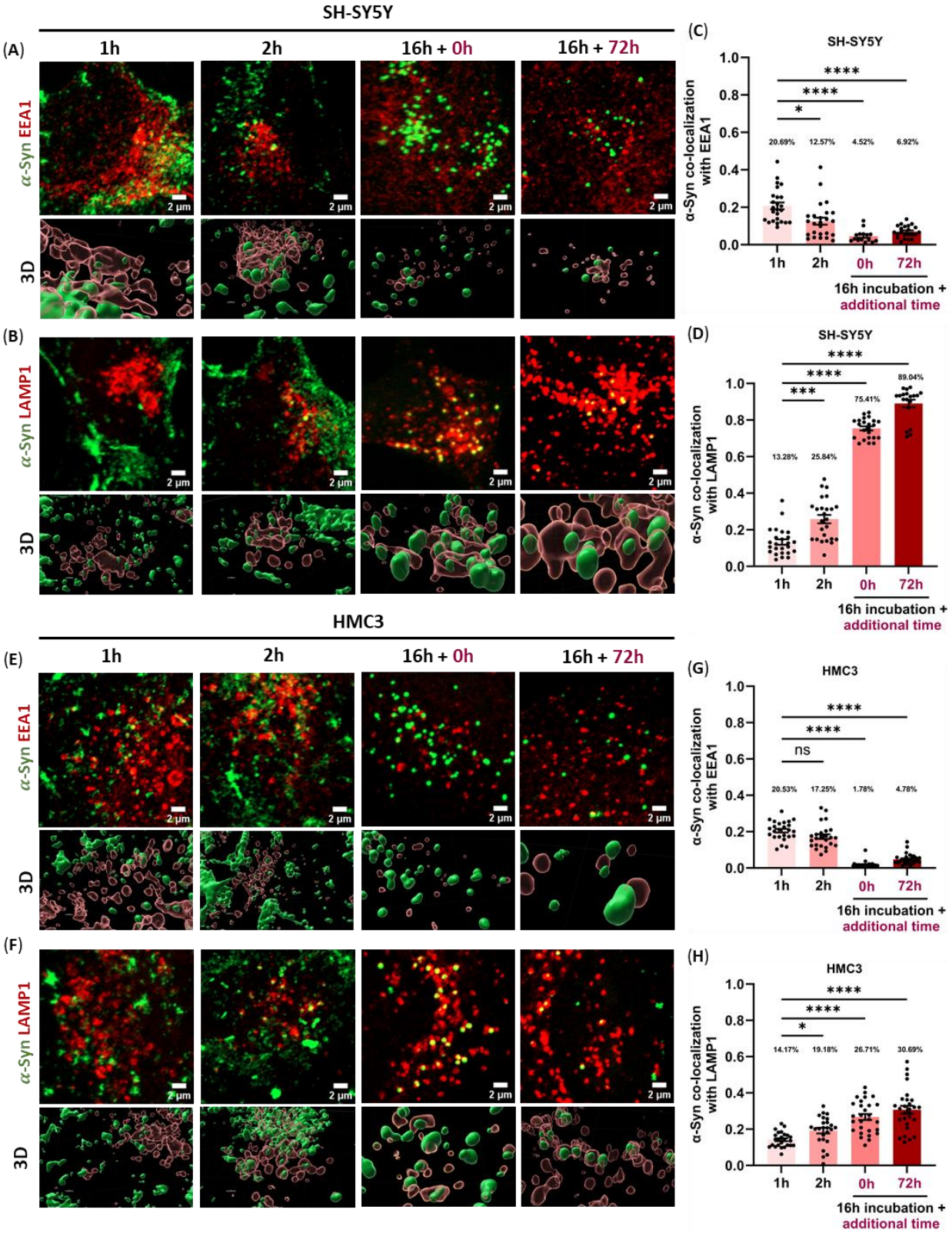

Figure 1. Spatio-temporal analysis α-Syn localization in neuronal cells and microglia. (**A**) Representative images of α-Syn localization with early endosomes in SH-SY5Y neuronal cells at different (indicated) time points. Imaris 3-D reconstructions (lower panels) are representative of different regions of interests. (**B**) Representative images of α-Syn localization with lysosomes in SH-SY5Y cells at different (indicated) time points. Imaris 3-D reconstructions (lower panels) are representative of different regions of interests. (**C**) Quantification of the extent of aggregates localized with early endosomes in SH-SY5Y cells. Co-localization represents Mander's Correlation Coefficient of the extent of α-Syn overlap with EEA1. (**D**) Quantification of the extent of aggregates localized with lysosomes in SH-SY5Y cells. Co-localization represents Mander's Correlation Coefficient of the extent of α-Syn overlap with LAMP1. (**E**) Representative images of α-Syn localization with early endosomes in HMC3 microglial cells at different (indicated) time points. Imaris 3-D reconstructions (lower panels) are representative of different regions of interests. (**F**) Representative images of α-Syn localization with lysosomes in HMC3 microglial cells at different (indicated) time points. Imaris 3-D reconstructions (lower panels) are representative of different regions of interests. (**G**) Quantification of the extent of aggregates localized with early endosomes in HMC3 cells. Co-localization is represented as Mander's Correlation Coefficient of the extent of α-Syn overlap with EEA1. (**H**) Quantification of the extent of aggregates localized with lysosomes in HMC3 cells. Co-localization is represented as Mander's Correlation Coefficient of the extent of α-Syn overlap with LAMP1. N=3 independent experiments for all groups. Data represented as mean ± SEM. Statistical significance was analyzed using Brown-Forsythe and Welch One-Way ANOVA with Dunnett's T3 multiple comparison. ns: non-significant, *$p<0.05$, ***$p<0.001$, ****$p<0.0001$.

Figure 2

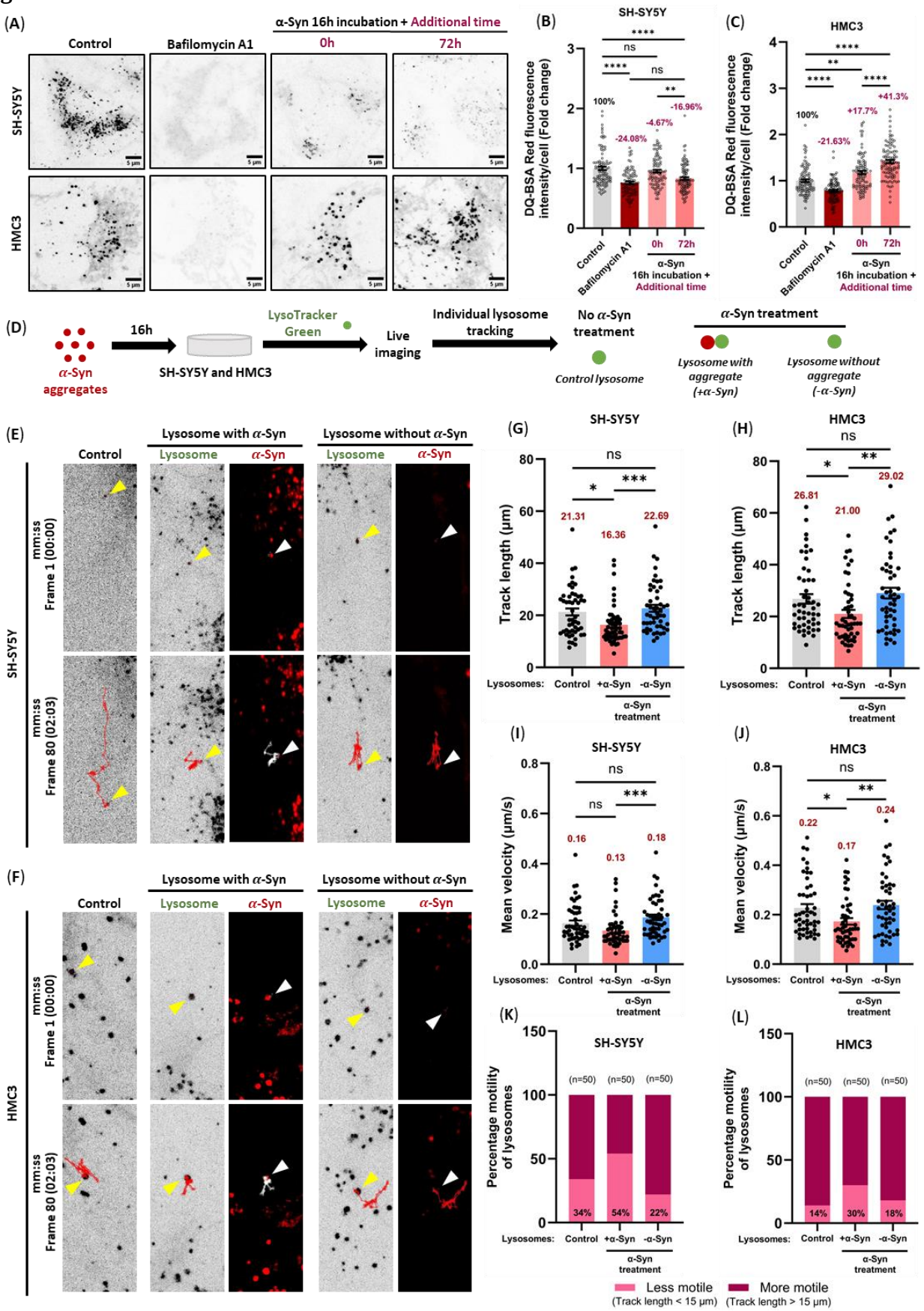
(A)
Control
Bafilomycin A1
α-Syn 16h incubation + Additional time
0h
72h
SH-SY5Y
HMC3
(B)
SH-SY5Y
DQ-BSA Red fluorescence intensity/cell (Fold change)
100%
-24.08%
-4.67%
-16.96%
Control
Bafilomycin A1
0h
72h
α-Syn 16h incubation + Additional time
(C)
HMC3
100%
-21.63%
+17.7%
+41.3%
(D)
α-Syn aggregates
16h
SH-SY5Y and HMC3
LysoTracker Green
Live imaging
Individual lysosome tracking
No α-Syn treatment
Control lysosome
α-Syn treatment
Lysosome with aggregate (+α-Syn)
Lysosome without aggregate (-α-Syn)
(E)
Control
Lysosome with α-Syn
Lysosome without α-Syn
Lysosome
α-Syn
mm:ss Frame 1 (00:00)
mm:ss Frame 80 (02:03)
(F)
(G)
SH-SY5Y
Track length (μm)
21.31
16.36
22.69
Lysosomes: Control +α-Syn -α-Syn
α-Syn treatment
(H)
HMC3
26.81
21.00
29.02
(I)
Mean velocity (μm/s)
0.16
0.13
0.18
(J)
0.22
0.17
0.24
(K)
Percentage motility of lysosomes
(n=50)
34%
54%
22%
(L)
14%
30%
18%
Less motile (Track length < 15 μm)
More motile (Track length > 15 μm)

Figure 2. Effect of α-Syn aggregates on lysosomal degradative ability and motility. (**A**) Representative images of DQ-BSA red fluorescence in different conditions for SH-SY5Y (upper panels) and HMC3 (lower panels) cells. (**B**) Fluorescence intensity quantification for SH-SY5Y cells. (**C**) Fluorescence intensity quantification for HMC3 cells. For both (**B**) and (**C**), N=3 independent experiments, n=100 cells per group. Data represented as fold change of control. Error bars represent SEM. Statistical significance was analyzed using Brown-Forsythe and Welch One-Way ANOVA with Games-Howell's multiple comparison. ns: non-significant, **p<0.01, ****p<0.0001. (**D**) Schematic representation of the experimental, and analysis strategy to track lysosome motility. (**E**) Representative images of the first frame (upper panels) and last (80th) frame (lower panels) of tracked lysosomes for SH-SY5Y cells. (**F**) Representative images of the first frame (upper panels) and last (80th) frame (lower panels) of tracked lysosomes for HMC3 cells. For both (**E**) and (**F**), arrowheads depict the tracked lysosome, with (white arrowheads) or without (yellow arrowheads) aggregates. (**G**) Mean track length of lysosomes in SH-SY5Y cells. (**H**) Mean track length of lysosomes in HMC3 cells. (**I**) Mean velocity of lysosomes in SH-SY5Y cells. (**J**) Mean velocity of lysosomes in HMC3 cells. For (**G-J**), mean values are mentioned in red within the graphs. (**K**) Proportion of lysosomes that travel less than 15 μm (less motile), or more than 15 μm (more motile) in different conditions for SH-SY5Y cells. (**L**) Proportion of lysosomes that travel less than 15 μm (less motile), or more than 15 μm (more motile) in different conditions for HMC3 cells. N=3 independent experiments, n=50 individual lysosomes tracked per group. Error bars represent SEM. Statistical significance was analyzed using Brown-Forsythe and Welch One-Way ANOVA with Games-Howell's multiple comparison. ns: non-significant, *p<0.05, **p<0.01, ***p<0.001.

Figure 3

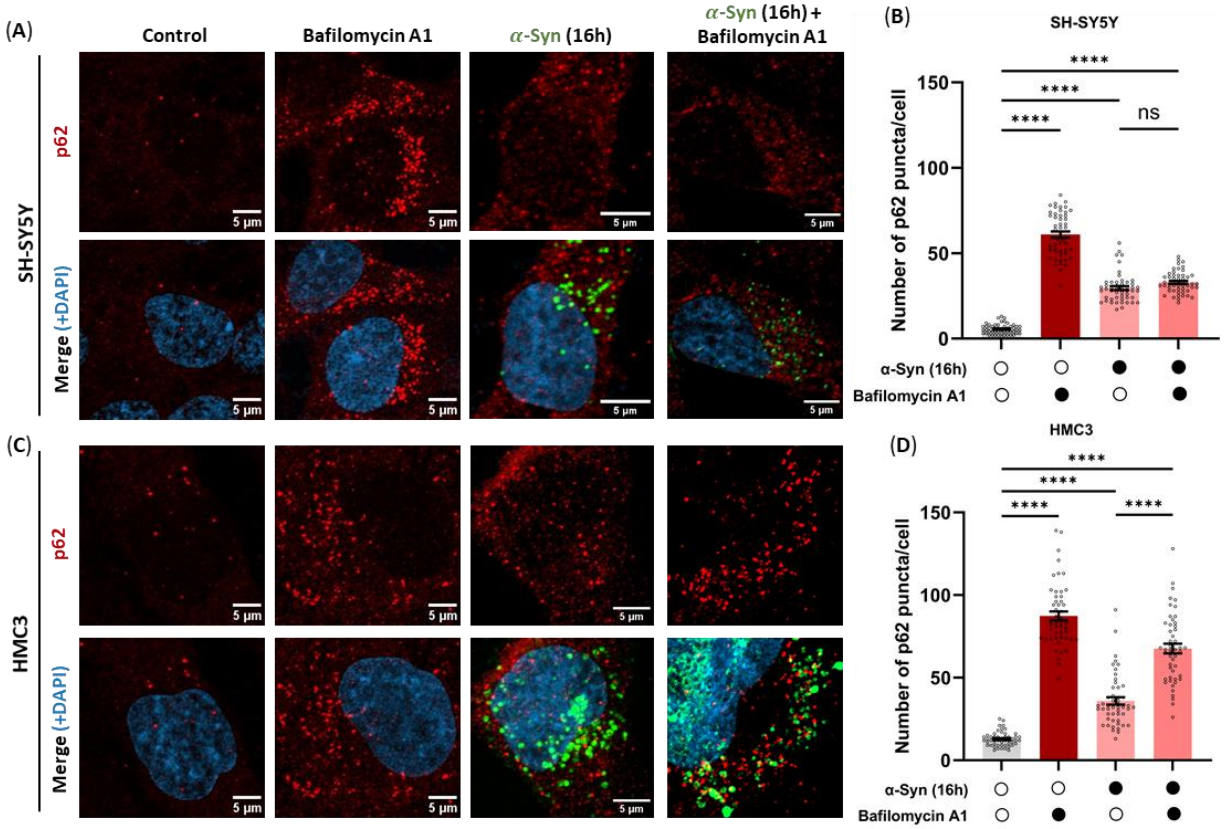

Figure 3. Effect of aggregates on autophagy flux. (**A**) Representative immunofluorescence images of p62 in the presence of α-Syn aggregates, with or without bafilomycin, in SH-SY5Y cells. (**B**) Corresponding quantification of the number of p62 puncta per cell for SH-SY5Y cells. (**C**) Representative immunofluorescence images of p62 in the presence of α-Syn aggregates, with or without bafilomycin, in HMC3 cells. (**D**) Corresponding quantification of the number of p62 puncta per cell for HMC3 cells. For both (**B**) and (**D**), N=3 independent experiments, n=50 cell per group. Error bars represent SEM. Statistical significance was analyzed using Brown-Forsythe and Welch One-Way ANOVA with Games-Howell's multiple comparison. ns: non-significant, ****p<0.0001.

Figure 4

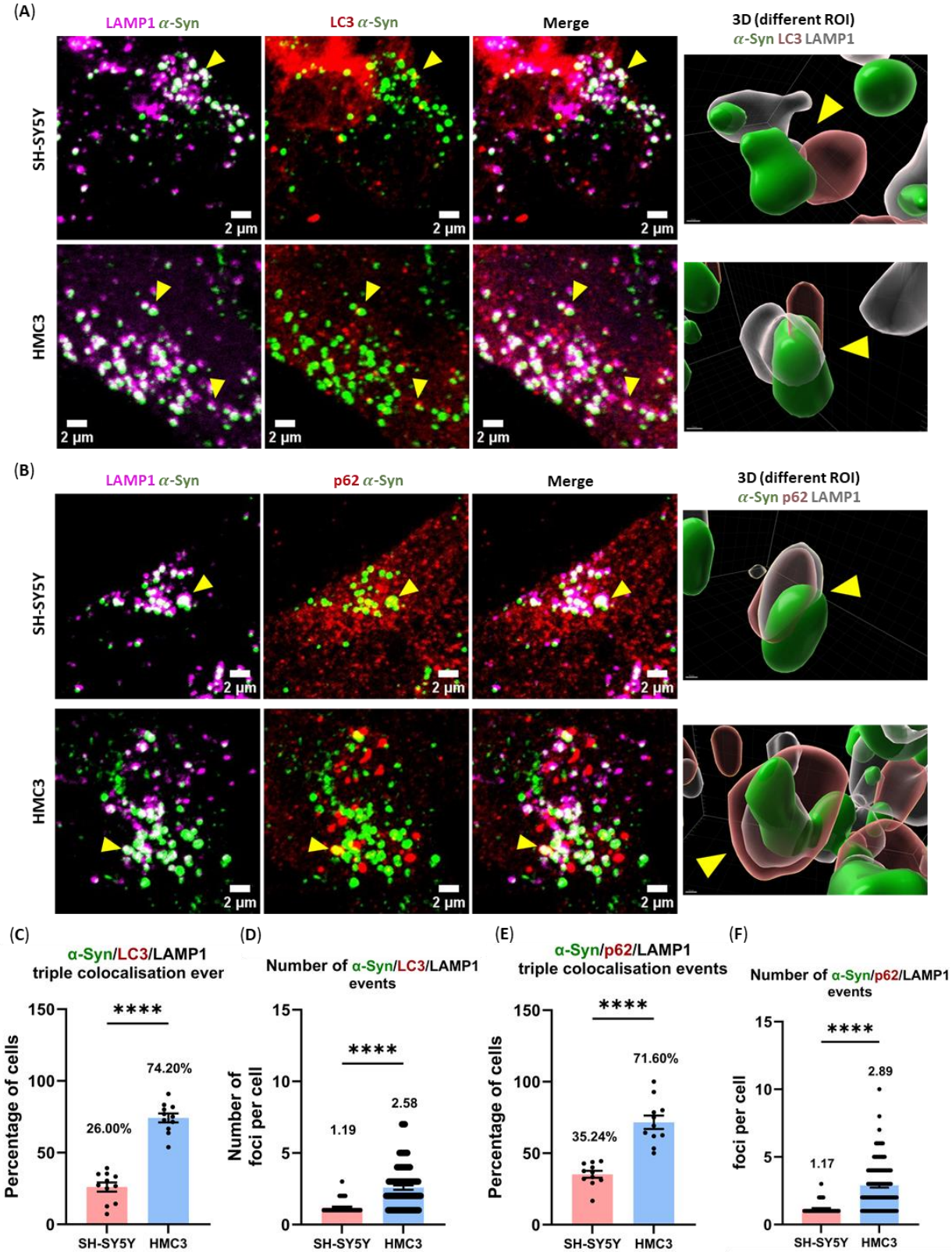
(A)
LAMP1 α-Syn
LC3 α-Syn
Merge
3D (different ROI)
α-Syn LC3 LAMP1
SH-SY5Y
HMC3
2 µm
(B)
LAMP1 α-Syn
p62 α-Syn
Merge
3D (different ROI)
α-Syn p62 LAMP1
(C)
α-Syn/LC3/LAMP1
triple colocalisation ever
Percentage of cells
****
26.00%
74.20%
(D)
Number of α-Syn/LC3/LAMP1
events
Number of
foci per cell
1.19
2.58
(E)
α-Syn/p62/LAMP1
triple colocalisation events
35.24%
71.60%
(F)
Number of α-Syn/p62/LAMP1
events
foci per cell
1.17
2.89
SH-SY5Y
HMC3

Figure 4. Triple colocalization events of aggregates, autophagy markers and lysosomes. (**A**) Representative immunofluorescence images of lysosomes (LAMP1) with LC3 and α-Syn in SH-SY5Y (upper panels) and HMC3 (lower panels) cells. Imaris 3-D reconstructions are from different regions of interests. Yellow arrowheads point towards the triple co-localized points. (**B**) Representative immunofluorescence images of lysosomes (LAMP1) with p62 and α-Syn in SH-SY5Y (upper panels) and HMC3 (lower panels) cells. Imaris 3-D reconstructions are from different regions of interests. Yellow arrowheads point towards the triple co-localized points. (**C**) Percentage of α-Syn-positive autolysosomes (with LC3 and LAMP1) in SH-SY5Y and HMC3 cells. Mean percentage is mentioned within the graph. N=3 independent experiments, number of cells analyzed: n=212 for SH-SY5Y and 133 for HMC3. (**D**) Average number of triple-colocalizing (aggregate with LC3 and LAMP1) foci per cell for SH-SY5Y and HMC3. Mean number of foci is mentioned within the graph. N=3 independent experiments, number of cells analyzed: n=56 for SH-SY5Y and 98 for HMC3 (cells positive for at least one triple colocalization event from [**C**]). (**E**) Percentage of α-Syn-positive autolysosomes (with p62 and LAMP1) in SH-SY5Y and HMC3 cells. Mean percentage is mentioned within the graph. N=3 independent experiments, number of cells analyzed: n=201 for SH-SY5Y and 155 for HMC3. (**F**) Average number of triple-colocalizing (aggregate with p62 and LAMP1) foci per cell for SH-SY5Y and HMC3. Mean number of foci is mentioned within the graph. N=3 independent experiments, number of cells analyzed: n=69 for SH-SY5Y and 109 for HMC3 (cells positive for at least one triple colocalization event from [**E**]). For (**C-F**), error bars represent SEM. Statistical significance was analyzed using unpaired Student's t-test with Welch's correction. ****$p<0.0001$.

Figure 5

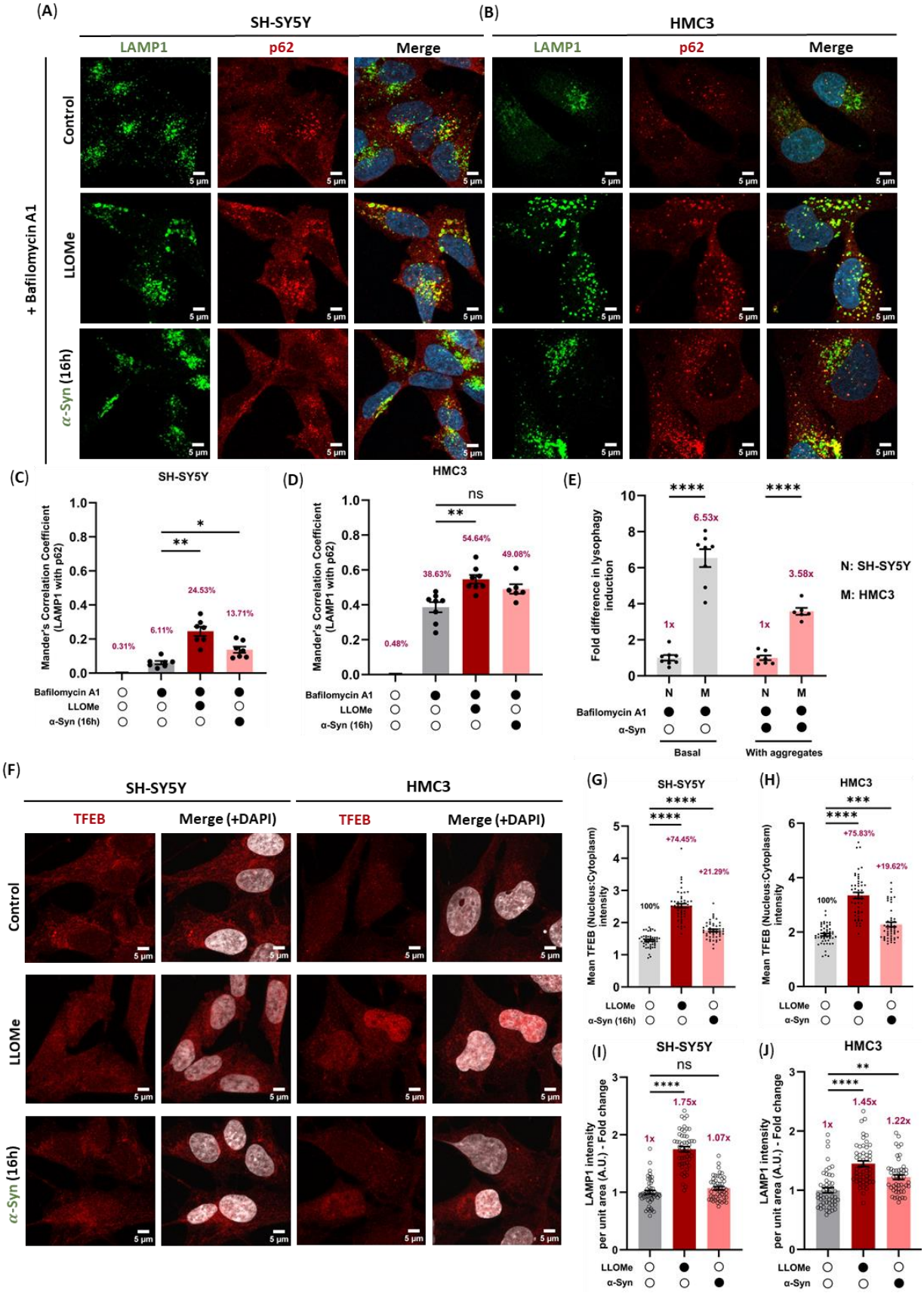
(A)
SH-SY5Y
LAMP1
p62
Merge
(B)
HMC3
+ Bafilomycin A1
Control
LLOMe
α-Syn (16h)
5 µm
(C)
SH-SY5Y
Mander's Correlation Coefficient (LAMP1 with p62)
0.31%
6.11%
24.53%
13.71%
Bafilomycin A1
LLOMe
α-Syn (16h)
(D)
HMC3
ns
0.48%
38.63%
54.64%
49.08%
(E)
Fold difference in lysophagy induction
6.53x
3.58x
1x
N: SH-SY5Y
M: HMC3
α-Syn
Basal
With aggregates
(F)
TFEB
Merge (+DAPI)
(G)
Mean TFEB (Nucleus:Cytoplasm) intensity
+74.45%
+21.29%
100%
(H)
+75.83%
+19.62%
(I)
LAMP1 intensity per unit area (A.U.) - Fold change
1.75x
1.07x
(J)
1.45x
1.22x

Figure 5. Effect of aggregates on lysophagy and lysosome biogenesis. **(A)** Representative images of SH-SY5Y cells immunostained for LAMP1 and p62 in the presence of bafilomycin A1. (**B**) Representative images of HMC3 cells immunostained for LAMP1 and p62 in the presence of bafilomycin A1. (**C**) Quantification of the extent of co-localization of LAMP1-positive structures with p62 as a readout for lysophagy in SH-SY5Y cells. Co-localization is represented as Mander's Correlation Coefficient of the extent of LAMP1 overlap with p62. Mean percentage of co-localization is mentioned within the graph. (**D**) Quantification of the extent of co-localization of LAMP1-positive structures with p62 as a readout for lysophagy in HMC3 cells. Co-localization is represented as Mander's Correlation Coefficient of the extent of LAMP1 overlap with p62. Mean percentage of co-localization is mentioned within the graph. For both (**C**) and (**D**), N=3 independent experiments. Error bars represent SEM. Statistical significance was analyzed using Brown-Forsythe and Welch One-Way ANOVA with Games-Howell's multiple comparison. ns: non-significant, *$p<0.05$, **$p<0.01$. (**E**) Comparative analysis of the fold-difference in lysophagy induction between neuronal (denoted as "N") and microglial (denoted as "M") cells. Fold difference is mentioned within the graph. Statistical significance was analyzed using Two-Way ANOVA with Šídák's multiple comparison. ****$p<0.0001$. (**F**) Representative images of TFEB immunostaining in SH-SY5Y (left panels) and HMC3 (right panels) cells in different conditions. (**G**) Quantification of the extent of TFEB translocation to the nucleus (mean TFEB intensity: nucleus-to-cytoplasmic ratio) in SH-SY5Y cells. Percentage increase relative to control is mentioned within the graph. (**H**) Quantification of the extent of TFEB translocation to the nucleus (mean TFEB intensity: nucleus-to-cytoplasmic ratio) in HMC3 cells. Percentage increase relative to control is mentioned within the graph. (**I**) Quantification of LAMP1 intensity per cell for SH-SY5Y, normalized to cell area. Data represented as fold change relative to control. Fold increase is mentioned within the graph. (**J**) Quantification of LAMP1 intensity per cell for HMC3, normalized to cell area. Data represented as fold change relative to control. Fold increase is mentioned within the graph. For (**G-J**), N=3 independent experiments, n=50 cells per group. Error bars represent SEM. Statistical significance was analyzed using Brown-Forsythe and Welch One-Way ANOVA with Games-Howell's multiple comparison. ns: non-significant, **$p<0.01$, ***$p<0.001$, ****$p<0.0001$.

Figure 6

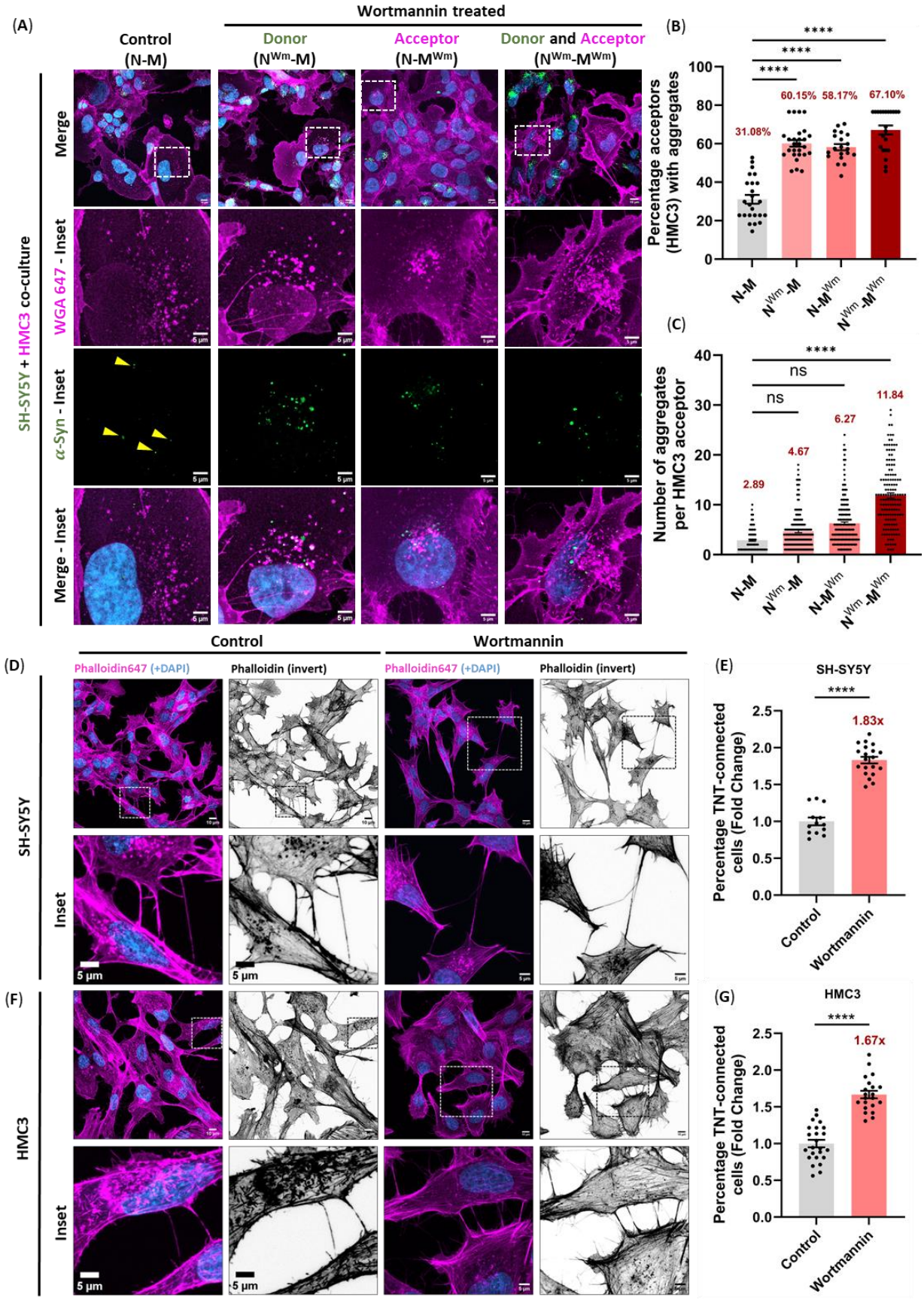
(A)
Wortmannin treated
Control (N-M)
Donor (N^{Wm}-M)
Acceptor (N-M^{Wm})
Donor and Acceptor (N^{Wm}-M^{Wm})
SH-SY5Y + HMC3 co-culture
Merge
WGA 647 - Inset
α-Syn - Inset
Merge - Inset
(B)
Percentage acceptors (HMC3) with aggregates
31.08%
60.15%
58.17%
67.10%
****
N-M
N^{Wm}-M
N-M^{Wm}
N^{Wm}-M^{Wm}
(C)
Number of aggregates per HMC3 acceptor
2.89
4.67
6.27
11.84
ns
(D)
Control
Wortmannin
Phalloidin647 (+DAPI)
Phalloidin (invert)
SH-SY5Y
Inset
5 µm
(E)
SH-SY5Y
Percentage TNT-connected cells (Fold Change)
1.83x
Control
Wortmannin
(F)
HMC3
(G)
HMC3
1.67x

Figure 6. Contribution of autophagy in transfer of aggregates, and its relation to TNTs. (**A**) Representative images of 12h co-cultures between α-Syn loaded SH-SY5Y neuronal cells and HMC3 microglia (control and wortmannin treated in different combinations). Wortmannin treatments of respective cell populations are represented by the superscript "Wm". Dotted box indicates the region zoomed in. (**B**) Percentage of HMC3 acceptor cells that received aggregates in control and wortmannin-treated cocultures. Average percentage of acceptor cells positive for aggregates mentioned in red within the graph. (**C**) Quantification of the number of aggregates received per cell by acceptor HMC3. Mean number of aggregates mentioned in red within the graph. For both (**B**) and (**C**), N=3 independent experiments. Error bars represent SEM. Statistical significance was analyzed using Brown-Forsythe and Welch One-Way ANOVA with Games-Howell's multiple comparison. ns: non-significant, ****$p<0.0001$. (**D**) Representative images of control (left panels) and wortmannin-treated (right panels) SH-SY5Y cells, stained for phalloidin. Dotted box indicates the region zoomed in. (**E**) Quantification of the percentage of connected cells, indicated as fold-change relative to control. Fold difference is mentioned within the graph in red. (**F**) Representative images of control (left panels) and wortmannin-treated (right panels) HMC3 cells, stained for phalloidin. Dotted box indicates the region zoomed in. (**G**) Quantification of the percentage of connected cells, indicated as fold-change relative to control. Fold difference is mentioned within the graph in red. For both (**E**) and (**G**), N=3 independent experiments. Statistical significance was analyzed using unpaired Student's t-test with Welch's correction. ****$p<0.0001$.